UV to Near-IR Emissions from C2H2 + O and C3O2 + O Flames at Low Pressure and High Temperature

1 November 1995

Prepared by

P. M. SHEAFFER, M. L. BURKE, and P. F. ZITTEL
Space and Environment Technology Center
Technology Operations

Prepared for

SPACE AND MISSILE SYSTEMS CENTER
AIR FORCE MATERIEL COMMAND
2430 E. El Segundo Boulevard
Los Angeles Air Force Base, CA 90245

Engineering and Technology Group

19960422 093

THE AEROSPACE CORPORATION
El Segundo, California

DTIC QUALITY INSPECTED 1

REPORT DOCUMENTATION PAGE

Form Approved
OMB No. 0704-0188

1. AGENCY USE ONLY (*Leave blank*)	2. REPORT DATE 1 November 1995	3. REPORT TYPE AND DATES COVERED

4. TITLE AND SUBTITLE

UV to Near-IR Emissions from C_2H_2 + O and C_3O_2 +O Flames at Low Pressure and High Temperature

6. AUTHOR(S)

Sheaffer, Patrick M.; Burke, Martin L.; and Zittel, Paul F.

5. FUNDING NUMBERS

F04701-93-C-0094

7. PERFORMING ORGANIZATION NAME(S) AND ADDRESS(ES)

The Aerospace Corporation
Technology Operations
El Segundo, CA 90245-4691

8. PERFORMING ORGANIZATION REPORT NUMBER

TR-95(5082)-1

9. SPONSORING/MONITORING AGENCY NAME(S) AND ADDRESS(ES)

Space and Missile Systems Center
Air Force Materiel Command
2430 E. El Segundo Blvd.
Los Angeles Air Force Base, CA 90245

10. SPONSORING/MONITORING AGENCY REPORT NUMBER

SMC-TR-96-08

11. SUPPLEMENTARY NOTES

12a. DISTRIBUTION/AVAILABILITY STATEMENT

Approved for public release; distribution unlimited

12b. DISTRIBUTION CODE

13. ABSTRACT (*Maximum 200 words*)

A spectroscopic study has been performed on the O + C_2H_2 combustion system in a high temperature, fast flow discharge system under highly dilute, fuel-lean conditions. Our previous work with room temperature flames has been extended to look for temperature-induced changes in the relative populations of CO(*a*), (*a'*), (*d*), and (*e*) reaction products by observing chemiluminescent emission in the 185–900 nm wavelength region at high temperatures. The effect of temperature on the relative yields of the CO triplet states was small, and the production rates increased linearly with the rate of the initial O + C_2H_2 reaction step. To test the importance of C_2O as a major pathway to triplet state CO, the results are compared to similar experiments run on the O + C_3O_2 system, which yielded a vibrationally hotter CO state distribution than O + C_2H_2. The overall temperature behavior of the O + C_3O_2 spectrum was significantly different from O + C_2H_2 and may be related to temperature variation of the branching ratio yielding C_2O in the initial reaction step. In addition, Cameron bands were observed at high temperatures (in order of decreasing relative intensity) when C_2H_4, C_2H_6, and CH_4 were used as fuels, and the Cameron band intensities displayed an unusual dependence on fuel concentration.

14. SUBJECT TERMS		15. NUMBER OF PAGES 39
Acetylene Cameron Bands Carbon Suboxide	Chemiluminescence Flame Spectra Ultraviolet	16. PRICE CODE

17. SECURITY CLASSIFICATION OF REPORT Unclassified	18. SECURITY CLASSIFICATION OF THIS PAGE Unclassified	19. SECURITY CLASSIFICATION OF ABSTRACT Unclassified	20. LIMITATION OF ABSTRACT

Acknowledgments

Contents

Figures

Table

1. Introduction

Emissions from electronically excited CO (CO*) are an important component of the emission spectra from low pressure hydrocarbon flames, but the chemical pathways from low molecular weight hydrocarbons to CO* are not fully understood. In our previous work, it was noted that although the Cameron CO($a{\rightarrow}X$), Asundi CO($a'{\rightarrow}a$), Triplet CO($d{\rightarrow}a$), and Herman CO($e{\rightarrow}a$) emission-band systems in hydrocarbon flames have been reported by several authors, not all band systems are consistently observed (Ref. 1). In that work, we quantified the CO* emissions from low pressure $C_2H_2 + O$ and $C_3O_2 + O$ flames at room temperature under highly dilute conditions and found that the CO(a) state was populated by radiative cascade from the higher lying triplet states, and that the relative state distributions of the Cameron, Asundi, Triplet, and Herman systems were nearly identical for both fuels. The latter observation indicates that a single chemical precursor is responsible for the formation of CO* in both fuels; however, it is not clear that this remains true at elevated temperatures. At higher temperatures, thermal energy may activate reaction pathways that are insignificant at room temperature, changing the elevated temperature CO* state distributions.

The primary thrust of this work is to examine the O atom combustion of acetylene and to extend our previous work on acetylene flames to elevated temperatures. This was done to search for reaction pathways that might not be significant at room temperature due to activation barriers. The reaction $C_3O_2 + O$ was also examined as a function of temperature since it appears that the source of CO* in this system,

$$C_2O + O \rightarrow CO + CO^*, \tag{1}$$
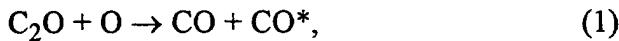
is also important in the production of electronically excited CO emissions when acetylene is burned in fuel-lean atomic oxygen flames (Refs. 1–6). Since the $C_2O + O$ reaction is the only viable path to populate CO* triplet states in the $C_3O_2 + O$ system, comparison of the temperature behavior of the emissions from the $C_3O_2 + O$ and the $C_2H_2 + O$ flames should yield valuable information on the nature of the CO* precursors in the $C_2H_2 + O$ reaction.

Burke et al. demonstrated, from the measured triplet CO* state distributions in low temperature C_2H_2 and C_3O_2 flames, that the CO(a) state was most likely populated via radiative cascade from the higher triplet states (Ref. 1). It was also pointed out that within the limits of experimental error, the relative populations of all triplet states (i.e., *a, a', d,*

and *e*) were the same for C_2H_2 + O and C_3O_2 + O flames. Thus, identical reaction mechanisms were inferred for the production of CO* emissions for both fuels, giving a strong indication that C_2O + O is the major reaction pathway in the C_2H_2 + O reaction system, at least at room temperature, as was inferred originally by Becker and Bayes (Ref. 4).

The C_2H_2 + O reaction process is complex, giving rise to several precursors that can lead to CO*:

$$CH + O \rightarrow CO^* + H \qquad \Delta H = -176 kcal/mol \qquad (2a)$$

$$CH_2 + O \rightarrow CO^* + H_2 \qquad \Delta H = -178 \ kcal/mol \qquad (2b)$$

$$C_2O + O \rightarrow CO^* + CO \qquad -181 \ kcal/mol < \Delta H < -200 \ kcal/mol \quad (2c)$$
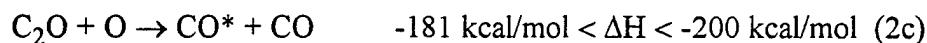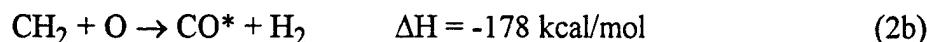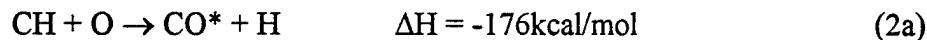
The C_2O in reaction (2c) may come predominantly from the reaction of O atoms with HCCO (Refs. 1,7), which appears to be formed with high yield in the primary O + C_2H_2 reaction step (Ref. 5). The reaction energies of (2a) and (2b) are insufficient to populate the CO(*e*) state, so Herman band emissions are not expected unless significant contribution from (2c) is present. It has been observed that the Herman system is extensively populated in acetylene combustion (Refs. 1, 4), which is consistent with reaction (2c) being the primary source of CO* in room temperature acetylene flames, although significant participation of (2a) and (2b) is not ruled out. It is therefore useful to compare the relative CO* state populations from both C_2H_2 + O and C_3O_2 + O flames, since reaction (2c) is the only viable source of CO* from C_3O_2.

An important consideration in the analysis of C_3O_2 + O emission spectra is the temperature dependence of the production of C_2O in the primary reaction step. Two major branches of the O atom reaction with carbon suboxide are (Refs. 8, 9)

$$C_3O_2 + O \rightarrow 3CO \qquad (3a)$$

$$C_3O_2 + O \rightarrow C_2O + CO_2. \qquad (3b)$$
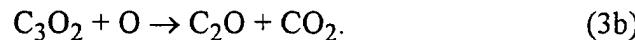
Pilz and Wagner (Ref. 8) saw little or no CO_2 in evidence as a gas-phase reaction product in their mass spectrometer measurement of the effluent of reaction (3) at moderately elevated temperatures. Since negligible amounts of CO_2 were observed in their apparatus, the branching ratio for reaction (3), $\beta = k_{3b}/k_{3a}$ is evidently very small, at least between 250 and 450 K. Also, Williamson and Bayes (Ref. 9) observed only an ~ 2%

yield of CO_2 for reaction (3b) in room temperature photolysis of dilute mixtures of N_2O and C_3O_2. The branching ratio, however, may be different at high temperatures.

In this work, we have extended the results obtained in a room temperature flame by Burke et al. to approximately 900 K, comparing the spectra of an acetylene-fuel flame with those of a carbon suboxide flame. We have also briefly examined other light hydrocarbon flames since C_2O has been detected in these systems (Ref. 2). Our experiments were performed under similar conditions to our previous work, but employ a better mixed sample and temperature control. All experiments were done in a fast-flow discharge system (FFDS) in order to provide a well-defined experimental system, as free as possible from the temperature, turbulence, and concentration gradients encountered in simple flames.

2. Experimental

2.1 Preliminary Considerations

Several unknowns complicate the data interpretation in this work. First, the CO(a) state is relatively long lived and is therefore strongly quenched in the FFDS by C_2H_2, O, O_2 (Ref. 10), and presumably also by C_3O_2, although no data appear to be available on the C_3O_2. The temperature dependencies of these quenching constants are unknown; however, since the room temperature quenching rate constants are near gas kinetic, we assume a temperature dependence proportional to the collision rate (i.e., $T^{1/2}$). Some uncertainty is therefore encountered in the extraction of CO(a) state populations, although the higher lying triplet states, CO(a', d, and e), radiate rapidly and so are largely unaffected by quenching. Second, the thermal stability of C_3O_2 is not clear, especially at temperatures above 450 K, so it was necessary to perform collateral mass spectroscopic studies to look for dissociation in the FFDS hot zone of dilute C_3O_2 at high temperature and in the absence of oxygen. Third, the branching ratio β for reaction (3) is not known as a function of temperature. Indeed, the primary differences in the temperature dependencies of the oxidation of C_3O_2 and C_2H_2 that was observed in this work may be the result of the temperature variation of this branching ratio.

2.2 Apparatus

Figure 1 shows a diagram of the heated flowtube system. A 1 × 1 in. square quartz tube was heated with heavy-duty nichrome heating tapes in two sections, upstream and downstream of the viewing region. The heaters were independently monitored and controlled by chromel-alumel thermocouples sandwiched between the tube and heating elements. The chemiluminescence signal was observed through the walls of the quartz flowtube, which were comparable in transparency to quartz optical windows. The spectrometer viewed the hot zone through calcium fluoride windows, which were installed to avoid localized convective cooling of the viewing region by the ambient atmosphere outside the tube.

5
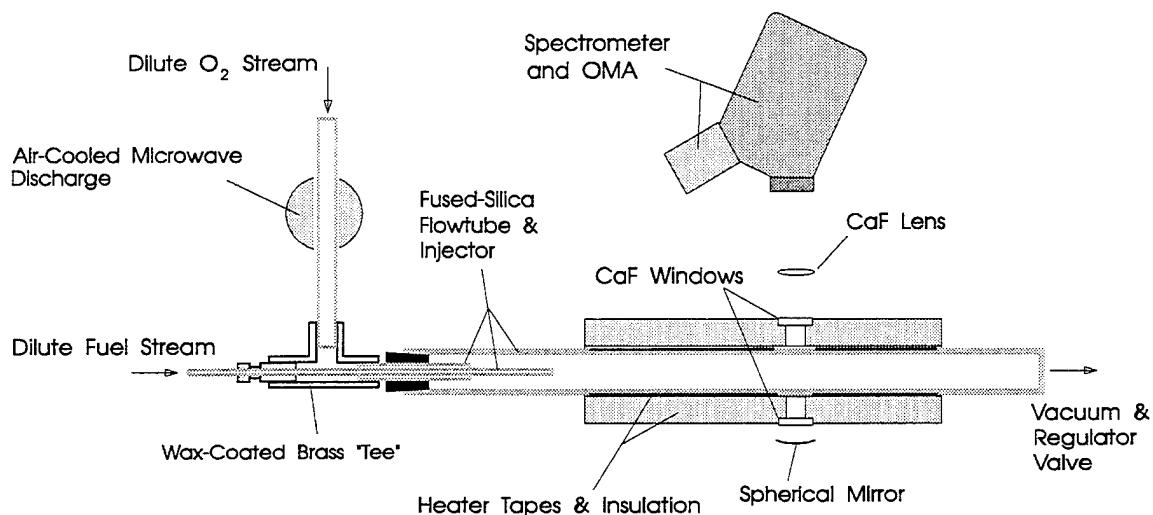
Figure 1. Diagram of fast flow discharge system.

The temperature in the hot zone was measured in the center of the tube with a sliding chromel-alumel thermocouple. The temperature varied linearly from room temperature at the start of the hot zone to 80% of the setpoint temperature after a distance of 6 cm, and achieved the setpoint temperature a short distance into the remaining 10 cm of the hot zone before the viewing region. For species density calculations, the above temperature profile was approximated by a step to the setpoint temperature located 6 cm into the hot zone.

The gas lines for the FFDS were all stainless steel, with stainless steel bellows valves. The dilution of some fuels was performed on a pressure basis with Celesco stainless steel differential electronic pressure gauges. The FFDS flowtube was entirely quartz, except for the joints near the microwave cavity. These joints were brass and rubber, but all areas exposed to the O atom flow were rendered inert by a heavy coating of halocarbon wax. It was found that an $O:O_2$ ratio of approximately 1 could be maintained for many weeks of continuous experimental time before it was necessary to replace the halocarbon wax.

One of the advantages of performing an FFDS experiment over other experimental arrangements is that the reactants are well thermalized and mixed by the time they reach the spectrometer view port, which may not be the case in experiments where the reactant mixing region and/or flame are directly viewed by the spectrometer. This advantage is important, because traces of nonthermalized species and unaccounted-for concentration gradients can give false indications of the temperature dependence of the reactions involved.

A 0.3 m f/5.3 McPherson folded-beam spectrometer was used to record the chemiluminescence signal through a 3.5 cm diam, f/5 calcium fluoride lens. Two different 1200 line/mm gratings were used to cover the spectral region from 185 to 900 nm, one blazed at 200 nm and the other at 500 nm. The beam-folding mirrors in the spectrometer were coated with LiF to maximize their UV reflectivity, and the spectrometer was continuously purged with dry nitrogen. The spectrometer was fitted with a Princeton Instruments optical multichannel analyzer (OMA), recording about 700 channels over an average 32.5 nm range. Continuous spectral plots were obtained by rotating the gratings 25 nm with a stepper motor under computer control between each exposure. The two gratings were manually interchanged at 325 nm. Two long-pass interference filters were inserted at the appropriate wavelengths to prevent interference from second order spectral components. Sixty spectra with fuel on and backgrounds with fuel off were taken for each run extending from 185 to 900 nm.

2.3   Chemical Sources

Matheson 99.994% purity argon was used as the buffer gas in this experiment. The acetylene was purchased as 2.0% in argon from Matheson. The CH_4, C_2H_4, and C_2H_6 were commercial purity and were diluted to 2.0% in argon in a clean 50 L stainless steel bomb prior to use. The carbon suboxide was prepared by dehydration of malonic acid with P_2O_5. The powders were mixed in the ratio 4:5 in a 1 L bulb, which was then connected to a Pyrex manifold, evacuated, and heated in a water-ethylene glycol bath to 130°C. The evolved gases were collected in a liquid-nitrogen-cooled ampoule, after which they were distilled and trapped in an ethanol slush bath. The trap was then pumped to approximately 3 Torr (to remove excess CO_2), valved off, and allowed to sublime into a 25 L bulb, yielding between 180 and 250 Torr of $C_3O_2 + CO_2$. The bulb was then filled with argon to about 800 Torr and connected to the FFDS fuel manifold. In our previous work, this method is known to yield C_3O_2 along with CO_2 at the level of

40% to 50% of the total (Ref. 1). However, the residual CO_2 may be considered to be an insignificant contributor with respect to combustion of fuels or quenching of CO(a).

All gas flows were metered through MKS, Inc., mass flow controllers. The O atom flows were generated using Matheson certified 5.0% oxygen in argon, which was further diluted with argon to 0.5% O_2 just before passing through the microwave discharge in a 12 mm diam quartz tube. The microwave discharge dissipated about 40 W. The O atom concentrations in the FFDS flowtube were determined before and after each run by titration with NO_2 (2.2% in argon), both upstream and downstream of the hot zone. A photomultiplier tube was located 30 cm downstream of the hot zone and was used to detect the titration endpoint. Typical O atom flows were 0.8 to 1.5 sccm in 560 sccm argon, with undissociated or recombined O_2 flows between 2.0 and 2.5 sccm. The fuel molecule flows were typically between 0.07 and 0.18 sccm, so that pseudo-first-order conditions in fuel were obtained. The total flowtube pressure in a typical run was 3 Torr.

2.4   Calibrations and Corrections

Since fuel and O atoms were partially consumed in the FFDS before reaching the spectrometer view port, it was necessary to correct the input flows to obtain the actual concentrations at the view port. The fuel concentrations at the spectrometer viewing region were determined from the initial flows and published values of the rate constants for (fuel) + O $\rightarrow$ (products). Table 1 shows the rate constant data used in this work (Refs. 10–12). The O atoms were in substantial excess and not significantly depleted by the fuel reaction. The total gas density and velocity in the flowtube were derived from flow measurements using absolute mass flow controllers (MKS, Inc.) and from the tube pressure and temperature. The velocity of the gas flow varied from 4 m/sec at room temperature to 12 m/sec at 873 K. At higher temperatures, the acetylene was consumed in the FFDS more rapidly than the associated increase in the gas flow velocity, so there was less fuel present at the spectrometer. However, with carbon suboxide, the decrease in dwell time in the hot zone (due to the increased flow velocity) dominated, and the fuel concentration at the spectrometer viewing region increased slightly at high temperature. Figure 2 shows the variation of all important species at the spectrometer viewing region as a function of temperature for typical sample flows.

It was also necessary to account for the quenching of CO(a) by other species in the flowtube. The radiative lifetimes of the a', d, and e states of CO are very short, on the order of 5 μsec (Ref. 10), allowing quenching of these transitions to be ignored.

Table 1. Rate Constant Data Used in Calculations

Reaction	E/R (K)	A (cc/mol. sec.)	Rate Constant
$C_3O_2 + O \rightarrow$ Products	1070	1.67×10^{-11}	$Ae^{-E/RT}$
$C_2H_2 + O \rightarrow$ Products	1794	6.19×10^{-11}	$Ae^{-E/RT}$
$CO(a) + M \rightarrow CO + M$[a]	---	2×10^{-10}	$A(T/295)^{1/2}$
$CO(a) + C_2H_2 \rightarrow CO + C_2H_2$	---	7.4×10^{-10}	$A(T/295)^{1/2}$

[a]M = O and O_2 have similar rate constants ($\pm 10\%$), and quenching by Ar was negligible (Ref. 10).
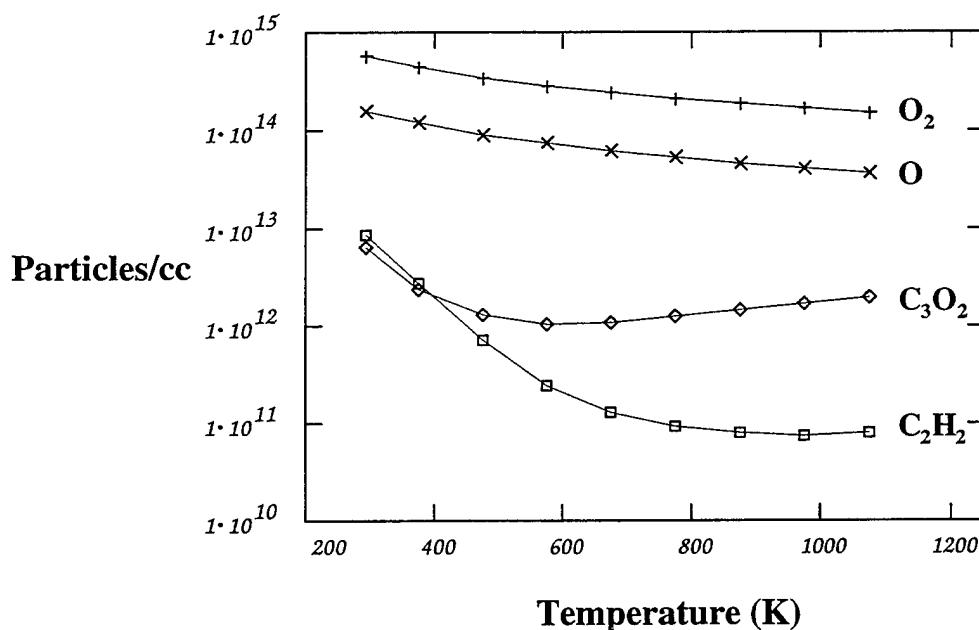

Figure 2. Species number densities at spectrometer viewing region for typical C_2H_2 and C_3O_2 flames as a function of temperature. Argon is not shown. The pressure is 3 Torr at all temperatures.

Quenching is, however, the dominant depopulation mechanism for the $CO(a)$ state, which strongly affects the observed intensity of the $a \rightarrow X$ Cameron transition (Refs. 1,10). The net quenching of the $CO(a)$ state by O, O_2 and fuel present at the spectrometer viewing region was calculated using literature values for the quenching constants at room temperature and the estimated temperature dependence (Table 1).

The relative sensitivity of the spectrometer as a function of wavelength was measured using a standard tungsten filament lamp that was calibrated to NIST data. The calibration curve was generated from 300 to 900 nm. The 185–300 nm range of the spectrometer was calibrated with a deuterium lamp and found to be relatively flat until near the 185 nm cutoff of the OMA.

Wavelength calibration of the spectrometer was carried out using a quartz-jacketed Hg pencil lamp in the ultraviolet (UV) and visible portions of the spectrum, and using argon emission lines from the plasma discharge in the near infrared (IR). The wavelength accuracy was better than ± 1 nm over the entire range from 185 to 900 nm.

It was not known whether C_3O_2 is stable at elevated temperatures. Pyrolysis of the C_3O_2 could yield products that could then react with O atoms to produce CO*, as well as alter the calculated fuel density in the spectrometer view port region. We therefore performed a mass spectrometric investigation on the argon-diluted fuel stream at high temperature with no O or O_2 present. An Extrel quadrupole mass spectrometer was connected to the flowtube 10 cm downstream of the hot zone via a length of fluoropolymer tubing. A separate vacuum pump located at the mass spectrometer was used to move the flowstream sample rapidly through the tubing, minimizing the loss of reactive species. The C_3O_2 signal on the mass spectrometer was observed to vary directly with the measured flow of fuel in the FFDS. When the flow was held constant and the FFDS heated, the C_3O_2 signal was observed to remain constant, even at temperatures up to 673 K, indicating excellent short-term stability for the C_3O_2, even in the presence of the hot quartz surfaces in the FFDS hot zone.

3. Results and Discussion

A comparison of spectral signatures and CO triplet state populations has been used in previous work to infer that the same reaction is responsible for CO* formation in C_3O_2 and C_2H_2 flames (Refs. 1, 4). Specifically, the $C_2O + O$ reaction appears to be the only viable source of CO* for the two fuels. It was also shown in previous work that within experimental error, the CO(a) state was populated predominantly by radiative emission from higher lying triplet CO states via the $a' \to a$, $d \to a$ and $e \to a$ transitions (Ref. 1). Essentially, the same vibrational state distributions were also observed for both fuels for the four triplet-state band systems that were seen. The previous observations were made in dilute low temperature flames. Here, we examine the temperature dependence of those observations. In particular, the possible occurrence of alternative sources of CO* at higher temperature, e.g., via $CH + O$ or $CH_2 + O$, was examined.

The CO emission bands observed for room temperature flames in previous work were practically identical for acetylene and carbon suboxide fuel systems (Ref. 1); however, in this work, we observed some important differences at elevated temperatures under very uniform flow conditions. Observations that we have made, which will be discussed in subsequent sections, include:

1. For the acetylene system, the intensities of all of the observed CO* band systems increase with temperature in quantitative accordance with the increase predicted by the $C_2H_2 + O$ reaction rate constant (Table 1).

2. The CO* spectrum for the carbon suboxide system exhibits a stronger temperature dependence than the acetylene system, and is nearly unobservable at room temperature. The temperature dependence cannot be accounted for with published kinetic data for the $O + C_3O_2$ reaction, and could be due to a strong temperature dependence for the branching ratio in reaction (3).

3. The higher vibrational bands of the Herman and Triplet systems are relatively brighter in the carbon suboxide flame than in the acetylene flame, indicating that the CO* is vibrationally hotter in the carbon suboxide system. This result is somewhat different than previous results in low temperature flames.

4. The intensities of the visible OH, CH, and C_2 emissions decrease quickly with increasing temperature relative to the triplet state CO* emissions in the acetylene system, and exhibit higher order kinetic behavior with respect to fuel.

5. The carbon suboxide system exhibits distinct CO Fourth Positive emission at all temperatures, whereas the acetylene system shows only traces of these emissions at low temperatures, which disappear altogether at higher temperatures.

11

3.1. Acetylene

When acetylene was used as fuel at room temperature, an elongated, diffuse, bright purple flame was observed, which extended downstream the entire length of the flowtube. At higher temperatures, essentially all the acetylene was consumed within the hot zone, so chemiluminescence was not observed in the flowtube after the hot zone.

The CO* band systems observed in the $C_2H_2 + O$ chemiluminescence spectrum are illustrated in Figures 3 and 4. The Cameron band system (CO $a{\to}X$) dominates the UV portion of the spectrum, although at low temperature, there is a trace of Fourth Positive emission between 185 and 193 nm. Between 280 and 450 nm, there were no emissions from CO* observed, but strong CH ($A{\to}X$) and ($B{\to}X$), as well as OH ($A{\to}X$) emissions, were observed. In the visible portion of the spectrum beyond 450 nm, the C_2 ($d{\to}a$) Swan bands are dominant. In the red and near-IR portions of the spectrum, the Herman, Triplet, and Asundi band systems are observed. For comparison, the plots in Figure 4 are offset and scaled so that the low-lying Triplet and Asundi bands are about the same size at the different temperatures. Note the dramatic relative decrease in the Swan band system between 460 and 520 nm as temperature is increased. Adjustment of the fuel flow at various temperatures, while still maintaining a significant excess of O atoms, yielded fuel reaction orders for the observed bands from electronically excited CO, CH, OH, and C_2. The CO* bands were all first order in fuel over the entire temperature range. The apparent reaction order of the CH, OH, and C_2 bands was significantly higher, and increased with temperature. The apparent order varied between 1 and 2 for OH ($A{\to}X$), and between 2 and 5 for CH ($A{\to}X$).

Total band system relative intensities as a function of temperature for the four CO* band systems observed here are shown in Figure 5. All band systems are complete, except for the Asundi system, which includes only the (4,0) and higher vibrational bands. At each temperature, the intensity data were corrected for reactant concentrations at the spectrometer viewing region, as well as for quenching of CO(a) in order to determine the relative production rate of each band system as a function of temperature. The spectra in Figure 5 have, however, been scaled before plotting in order to allow comparison. The Triplet, Cameron, and Asundi band systems have a very similar temperature dependence. The decrease in intensity of the Herman bands at higher temperatures may be the result of incompletely resolving the Herman from the C_2 Swan band system, which decreases in intensity dramatically as the temperature increases.

12
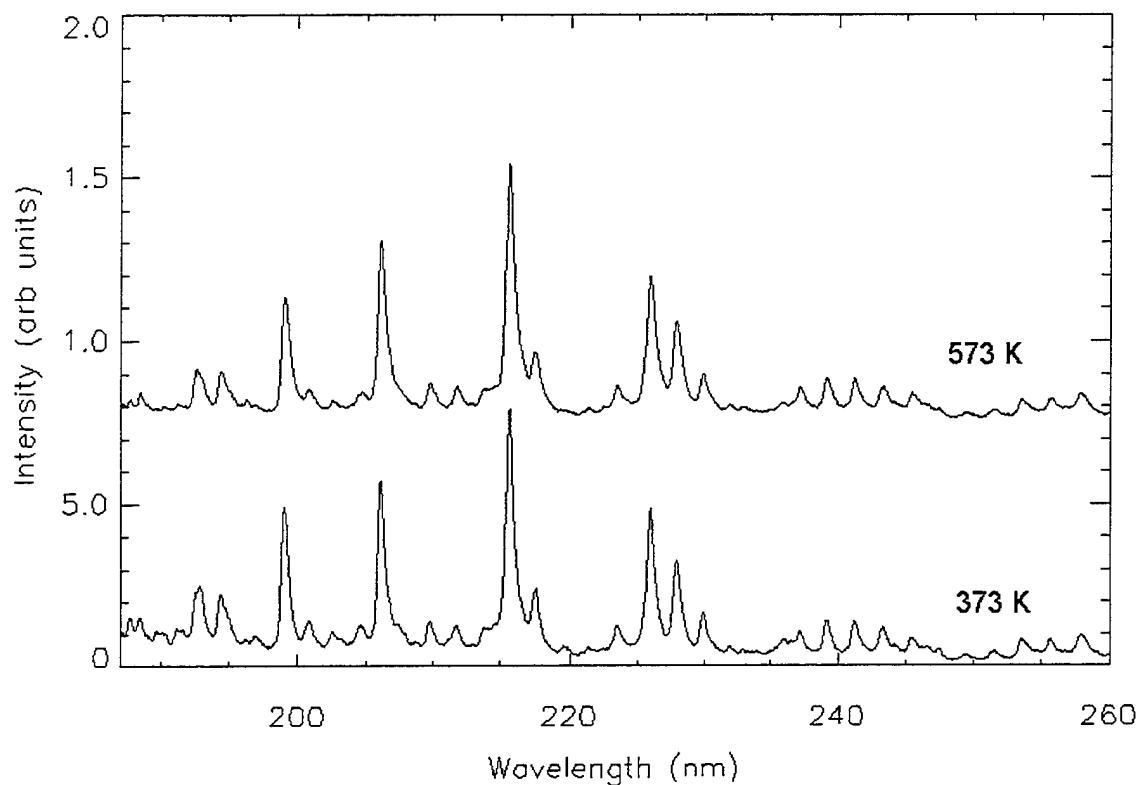
Figure 3. Ultraviolet emission spectra of C_2H_2 + O flame, showing Cameron band emissions, as well as Fourth Positive emissions below 195 nm. For comparison, the plots have been offset and scaled to yield the same overall intensity and are corrected for spectrometer sensitivity.
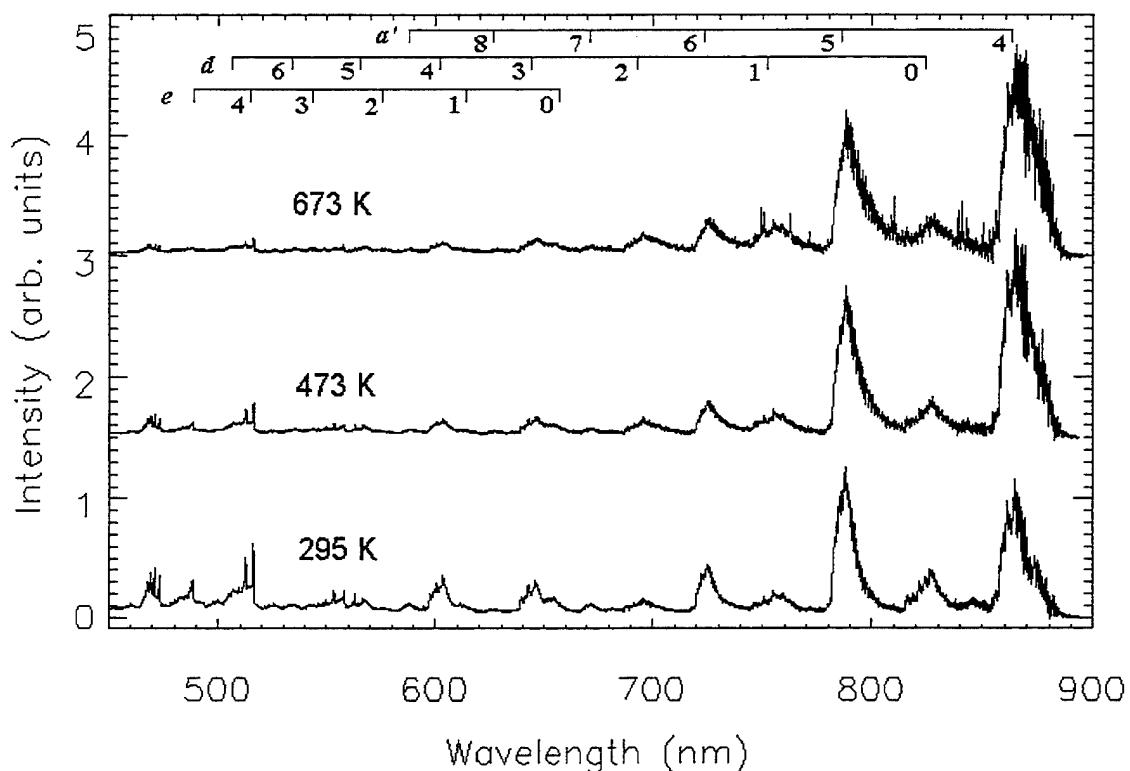
Figure 4. Visible/IR emission spectra of C_2H_2 + O flame, showing Triplet and Asundi bands, as well as C_2 Swan bands. For comparison, the plots have been offset and scaled to yield the same approximate intensity for the lower Triplet and Asundi bands. Spectra have been corrected for relative wavelength sensitivity of the spectrometer. The (v',0) vibrational assignments for the $a' \rightarrow a$, $d \rightarrow a$, and $e \rightarrow a$ transitions are shown.
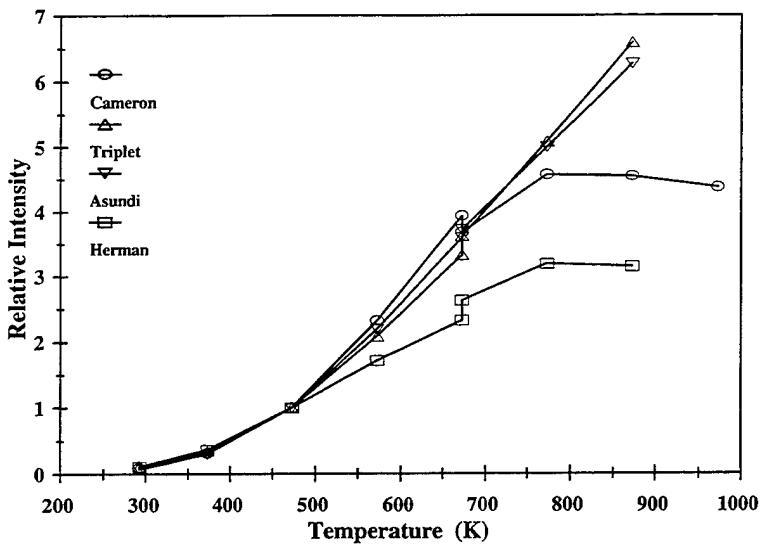
Figure 5. Total relative band system intensities for Cameron, Herman, Asundi, and Triplet bands in acetylene flame as a function of temperature. Relative intensities are normalized to 1 at 473 K.
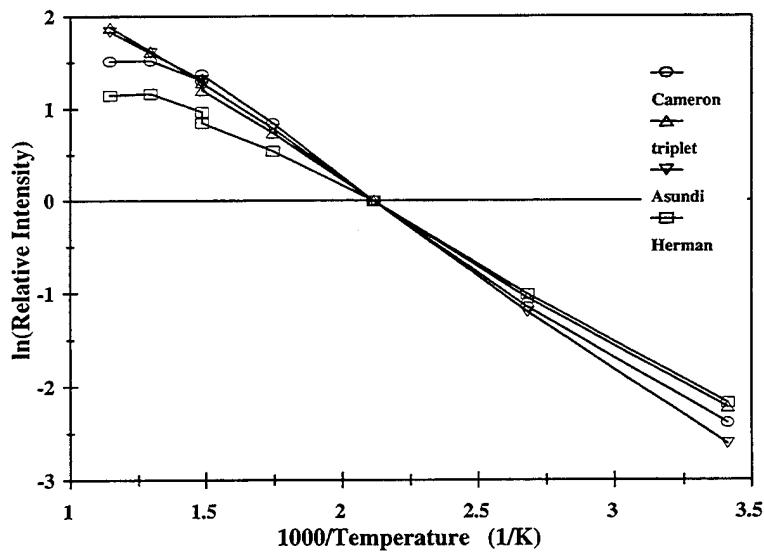
Figure 6. Arrhenius plot of relative band intensity vs temperature for acetylene flame. Relative intensities are normalized to 1 at 473 K.

Figure 6 is an Arrhenius plot of the band intensity data for the acetylene + O reaction. The range of activation temperature values that fits the Cameron, Triplet, and Asundi band emission data is E/R = 1750 ± 250 K. This result agrees well with the value in Table 1 for the activation temperature of the first reaction step, C_2H_2 + O → products. The agreement between the temperature variation of the total intensity of the Triplet and Asundi bands, which are not quenched, and that of the Cameron bands, which are strongly quenched, supports the accuracy of the correction procedure for CO(a) quenching.

The data are most simply interpreted to suggest that the temperature dependence of the intensity of all of the triplet CO* emission systems is due to the temperature dependence of the primary C_2H_2 + O reaction step, and that the subsequent steps to produce CO* are relatively independent of temperature as to CO triplet state distributions. The subsequent steps that are expected to generate CO* are very fast and are unlikely to limit the production rate of CO*. The chemical branching ratios leading to different CO electronic states could, however, have a temperature dependence, but the data suggest that it is not significant. The simplest explanation of the results is that the same reaction sequence is dominant over the whole temperature range of these experiments and that the branching ratios to CO triplet states in the final reaction step are relatively temperature independent. These observations, when combined with the conclusions of other work regarding the C_2O intermediate (Refs. 1, 4, 6), suggest the conclusion that under dilute, fuel-lean conditions, C_2O is the major precursor to CO* over a broad range of temperature for the C_2H_2 + O flame system.

3.2. Carbon Suboxide

When C_3O_2 was used as fuel, spectra similar to those obtained with C_2H_2 were recorded. The brightness of the flame *in the hot zone* increased dramatically as the temperature was increased, unlike the acetylene flame, which did not appear to increase significantly in intensity at higher temperatures. It was difficult to obtain carbon suboxide flame spectra below about 375 K, since integration times exceeded 24 hr for even marginally satisfactory spectra under fuel-lean conditions. Figures 7 and 8 show typical high temperature carbon suboxide flame spectra in the UV and visible/near IR regions, respectively.

The CO* triplet state distributions appear to be vibrationally hotter than for the C_2H_2 flame. This is particularly evident for the d and e states (i.e., Triplet and Herman systems).
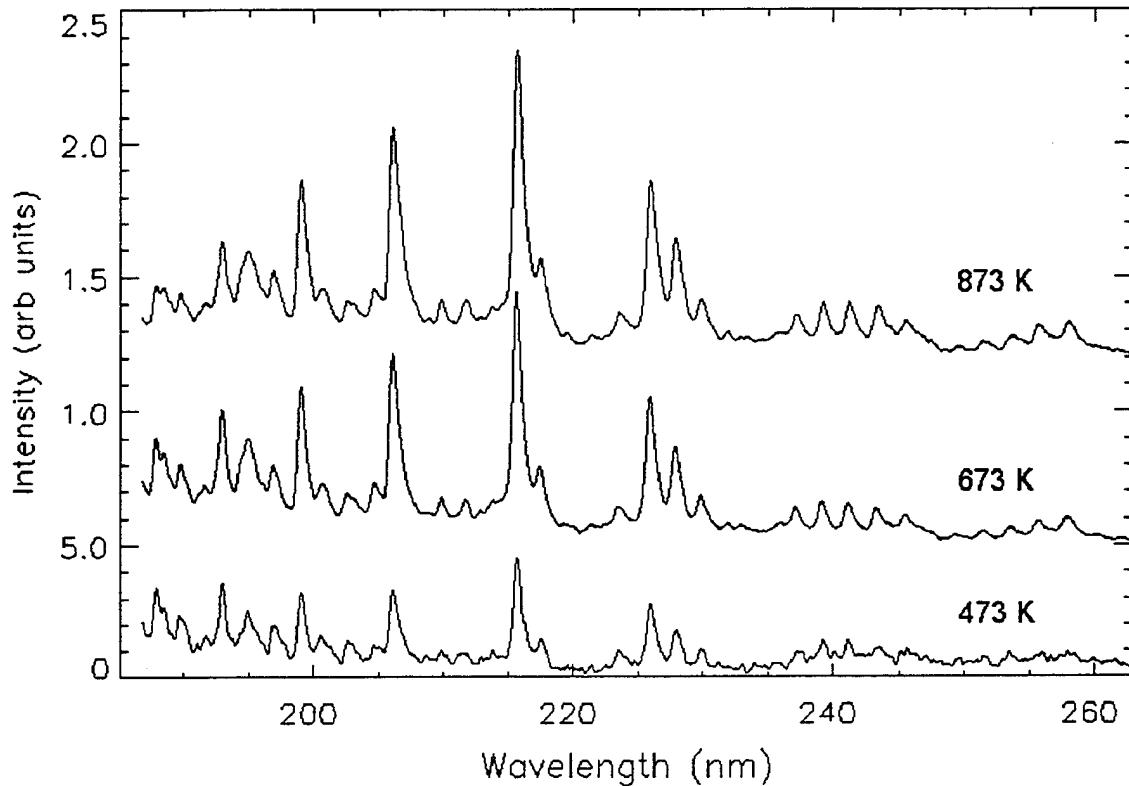
Figure 7. Typical UV spectra from C_3O_2 flame at elevated temperatures. Spectra are scaled and offset to the same approximate total intensity. Spectra have been corrected for spectrometer sensitivity.
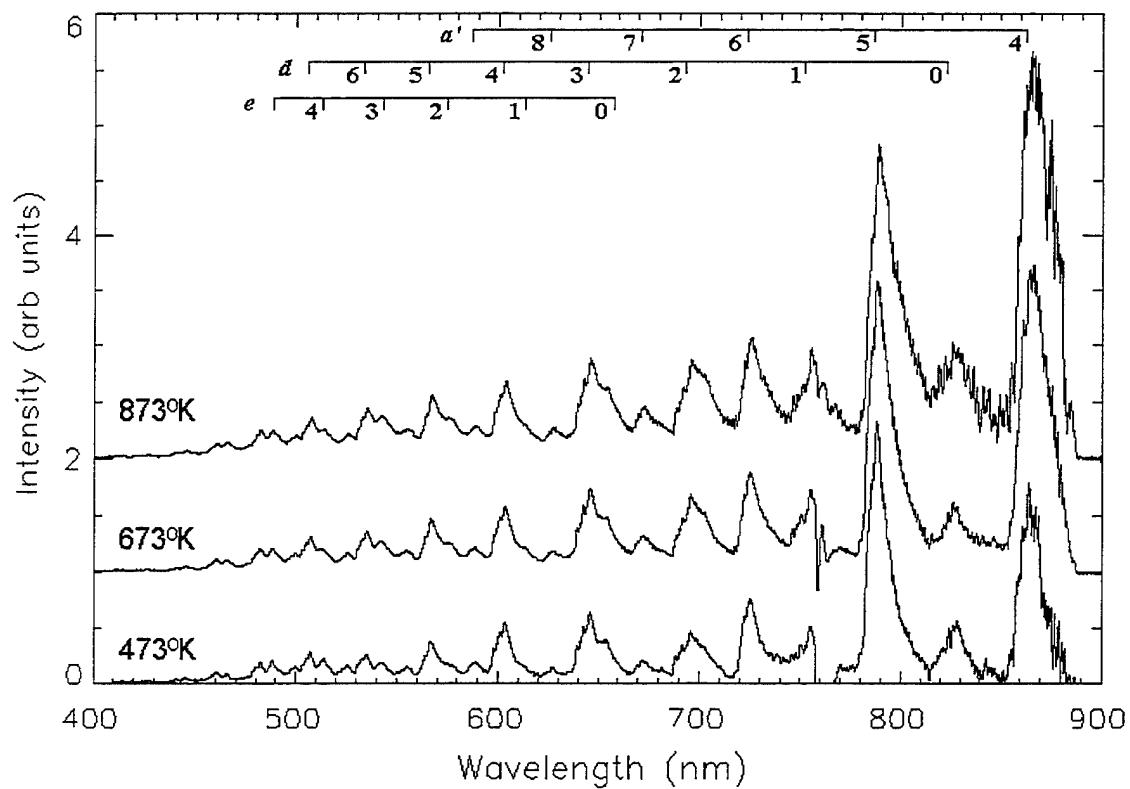
Figure 8. Typical visible/near-IR spectra from C_3O_2 flame at elevated temperatures. Spectra are scaled and offset to the same approximate total intensity. Spectra have been corrected for spectrometer sensitivity. The (v',0) vibrational assignments for emission from the $a' \rightarrow a$, $d \rightarrow a$, and $e \rightarrow a$ transitions are shown.

Although slightly obscured by overlap with the CH and C_2 systems in the acetylene spectra (Figure 4), the higher vibrational bands of the Triplet and Herman systems appear significantly more pronounced compared to the lower vibrational bands in the carbon suboxide spectra (Figure 8) than they are in the acetylene spectra. A vibrationally hotter CO* state distribution may result from the participation of vibrationally excited C_2O in reaction (1), as has been previously suggested (Refs. 1, 3). The C_2O may be more highly vibrationally excited in the carbon suboxide system due to the higher exothermicity of the C_3O_2 + O reaction, compared with the reaction that generates C_2O in the acetylene flame. The extra internal energy may be passed to CO* in the subsequent C_2O + O reaction. This is also reflected in the Fourth Positive bands seen just above the 185 nm cutoff of the OMA in the carbon suboxide spectra, which are only just barely observable in the low temperature acetylene spectra. The excess energy in the carbon suboxide reaction may populate the CO(A) state via intersystem crossing (Ref. 7).

Of interest is the behavior of the O_2 $b \rightarrow X$ emission feature at 762 nm. This emission did not appear in any of the C_2H_2 + O experiments. It is also completely quenched by the presence of C_3O_2, or C_3O_2-generated radicals, because it appears only in the *background* C_3O_2 + O spectra. The feature is therefore inverted in Figure 8, which is background subtracted, like all other spectral plots . A second point is that it also appears to be quenched by wall reactions. This deduction results from the observation that the O_2 $b \rightarrow X$ emission did not appear in initial spectra taken with C_3O_2 fuel, but gradually appeared only after several C_3O_2 + O spectra were taken. This indicates that the walls of the flowtube were gradually changed by the C_3O_2 flame, and no longer quenched $O_2(b)$. The increased vibrational temperature of the CO* spectra of the C_3O_2 flame was not related to the presence or absence of the O_2 $b \rightarrow X$ emission.

At room temperature, no detectable spectra were obtained with the carbon suboxide fuel, even for long integration times. Cameron band emission from C_3O_2 + O under dilute conditions became observable, beginning at a temperature of approximately 350 K. Above 350 K, the increase in CO* emission intensity was dramatic. This behavior cannot be accounted for with the published rate constant data for the C_3O_2 + O primary reaction. For example, decreasing the temperature below 350 K slightly increases the number of fuel molecules and O atoms in the viewing region of our apparatus (see Figure 2), and slightly decreases the C_3O_2 + O reaction rate constant, resulting in a very small net effect on the predicted reaction rate. The emission decreases substantially, however, on decreasing the temperature below 350 K. It is possible that the temperature dependence of the C_3O_2 + O

reaction rate constant (Table 1) is underestimated. A second possibility, however, is that the reported small branching ratio β in reaction (3) (Refs. 8, 9) may be a stronger function of temperature than the rate constant for the primary $C_3O_2 + O$ reaction.

Figure 9 shows the increase in total band system intensity with temperature for the important CO* emissions for the $C_3O_2 + O$ flame. The data were analyzed in the same way as the acetylene spectra, using the same band integrations. The plots are not as smooth as those for acetylene, probably due to batch-to-batch variations in C_3O_2 synthesis yield. An activation temperature (E/R) specifically for the production of CO* can be calculated from the temperature dependencies of the relative band intensities for emissions from the higher triplet states of CO, which radiate rapidly enough that quenching is negligible. The value calculated from the Arrhenius plot in Figure 10 is E/R = 2700 ± 400 K in the temperature range from approximately 500 to 800 K. The uncertainty in this calculation is fairly significant due to uncertainty in the actual fuel concentration at the spectrometer view port, which was calculated using the rate constant for the reaction, $C_3O_2 + O \rightarrow$ products. The activation temperature that was found for the CO* emission is much greater than for the primary reaction, $C_3O_2 + O \rightarrow$ products (Table 1). One explanation is the possibility of a large activation barrier, and consequent large temperature dependence, for the channel that produces C_2O. Since the activation temperature is also much larger than that observed for CO* emission from $C_2H_2 + O$, it is unlikely that the calculated activation temperature is associated with the $C_2O + O$ reaction. It is also not clear why the band system intensity of the Cameron bands appears to increase more rapidly than the Herman, Triplet, and Asundi bands. It is unlikely that this indicates a difference in the quenching of CO(a) by C_2H_2 and C_3O_2, but may suggest the thermal activation of a minor chemical pathway that populates CO(a) directly in the $C_3O_2 + O$ flame.

3.3.   Comparison of $C_2H_2 + O$ and $C_3O_2 + O$ Flame Spectra

The emission spectra of C_2H_2 and C_3O_2 flames are very similar. The relative vibrational populations of the CO(a) state for these fuels are identical (Figures 3 and 7), although Fourth Positive emissions are additionally present in the carbon suboxide spectra. On the other hand, the CO a', d, and e relative state populations appear vibrationally hotter in the $C_3O_2 + O$ flame spectra. The difference between the Cameron emission and the other triplet emissions may reflect the different dominant population mechanisms of the triplet states. The CO(a) state appears to be populated almost entirely via radiative
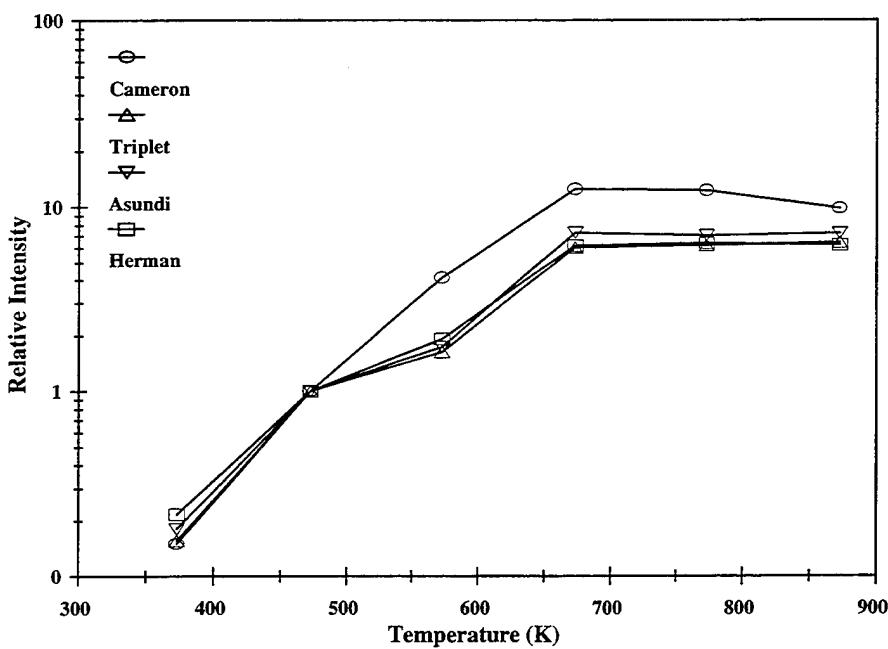
Figure 9. Band system relative intensity data for carbon suboxide flame.
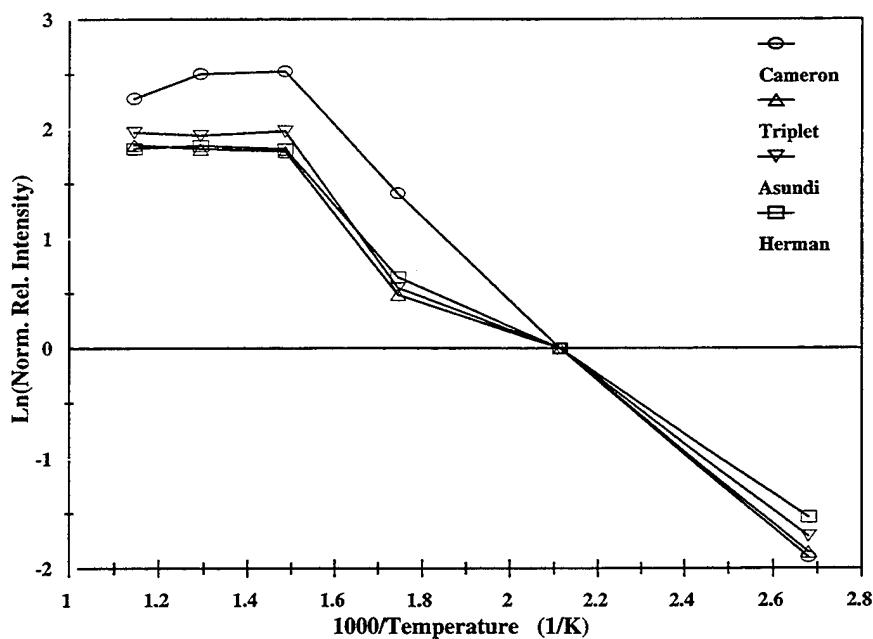
Figure 10. Arrhenius plot of relative band intensity data vs temperature for carbon suboxide flame.

emission from higher triplet states involving highly nondiagonal Frank-Condon factors. The resulting vibrational distribution in the *a* state may not reflect very strongly the distributions in the upper electronic states of the radiative transitions. The *a'*, *d*, and *e* states, however, are populated directly in the chemical reaction, and thus their vibrational distributions would be more sensitive to the vibrational temperature of the precursor, C_2O. The presence of the CO *A→X* Fourth Positive emission is consistent with this explanation, since these emissions also may reflect vibrationally hotter C_2O and a correspondingly hotter nascent vibrational population of CO* in the C_3O_2 flame. The CO(*A*) state is apparently populated via intersystem crossing from the high-lying triplet states (Ref. 7), and only CO(*e*) and CO(*d*, v > 3) states are energetic enough for this transfer to occur (Ref. 13).

Figures 4 and 8 show that the same CO* triplet-to-triplet band systems are present with both fuels in the visible and near-IR portions of the spectrum. In both cases, the lower-lying Asundi bands are predominant. Since Herman bands are present in both fuels, a highly exothermic reaction is indicated in order to populate the observed CO(*e*) levels. The lower exothermicity of reactions (2a) and (2b) seems to preclude formation of an extensive CO(*e*) population, which is consistent with the assertion that reaction (2c) is the major source of CO* in these systems.

In order to compare the triplet state vibrational distributions for acetylene and carbon suboxide flames, the (v',0) vibrational bands within a given band system were integrated and converted to a relative upper vibrational level population according to the equation,

$$P_{v'} = I_{v',0} \left[\frac{v_{v',0}^3 q_{v',0}}{\sum\limits_{v''} v_{v',v''}^3 q_{v',v''}} \right]^{-1}$$

where $P_{v'}$ is the relative vibrational state population of the upper level, $I_{v',0}$ is the integrated intensity of the (v',0) transition, $v_{v',v''}$ is the frequency of the (v',v'') transition, $q_{v',v''}$ is the Frank-Condon factor, and the sum is over all lower states, v''. For comparison, these populations were then normalized to the (5,0) band result in the Asundi system and to the (0,0) band result in the Triplet system. The (4,0) Asundi band was close to the OMA cutoff wavelength, resulting in more uncertainty in the relative population of the *a'*, v = 4 level.

Figures 11 and 12 show the relative vibrational state populations of the CO a' and d levels, respectively, for both the acetylene and carbon suboxide flames. The higher vibrational bands of the Asundi and Triplet systems, as well as the entire Herman system, were not included, due to overlap with other CO* emissions and, for the acetylene flame, with C_2 Swan bands. Nonetheless, it can be seen that in all cases, the CO* appears vibrationally hotter in the carbon suboxide flame than in the acetylene flame. The vibrational distributions appeared relatively constant over the temperature range investigated for the Triplet and Asundi systems. Therefore, the data from all temperatures were pooled, and the data in these figures represent *average* relative population distributions over the temperature range investigated (i.e., 473–873 K).

In contrast to our previous work performed with a different flow system (Ref. 1), it is noted that we were not able to observe CO* emissions from a C_3O_2 flame *at room temperature* under fuel-lean conditions in this FFDS. In the previous experiments, chemiluminescence spectra were recorded for a region 1–3 cm downstream of the point of mixing of the fuel and O atom streams. We therefore performed additional room temperature experiments in the present FFDS with the injector positioned about 1 cm upstream of the spectrometer viewing region, instead of at the normal position just before the hot zone (i.e., 16 cm upstream of the spectrometer viewing region). With carbon suboxide as fuel in this configuration, and at the same flows as in other experiments reported here, the entire spectral signature of CO* was very easily observed at room temperature, as depicted in Figures 13 and 14. The Triplet vibrational bands at 605 and 650 nm are also more pronounced than immediately adjacent Triplet and Asundi bands, in contrast to our other C_3O_2 spectra (see Figure 8), and are similar in this respect to both the acetylene and carbon suboxide spectra observed previously (Ref. 1). The CO(a') and (d) vibrational populations derived from the experiment with the injector 1 cm upstream of the spectrometer are included in Figures 11 and 12.

The reason for the brighter emission spectrum near the injector tip is not entirely clear. Since the concentration of fuel molecules and O atoms along the length of the flowtube at room temperature is fairly constant, there must be some nonequilibrium conditions near the tip of the injector that yield an increased reaction rate. The injector surface may catalyze the recombination of O_2 or quenching of $O_2(b)$, both of which may propagate energy into the fuel stream, increasing reaction rates in general and/or favoring

23
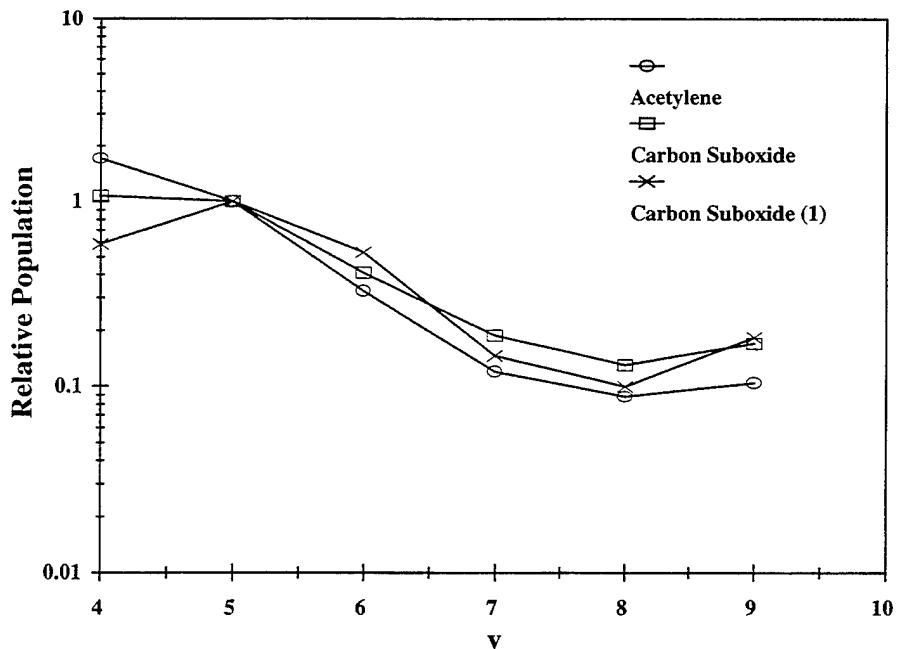
Figure 11. Relative vibrational state populations of CO(a') typical of the 473–873 K temperature range. The carbon suboxide fuel yields a slightly hotter vibrational state distribution than the acetylene fuel. "Carbon suboxide (1)" refers to the result at room temperature with the view port 1 cm downstream of the injection point.
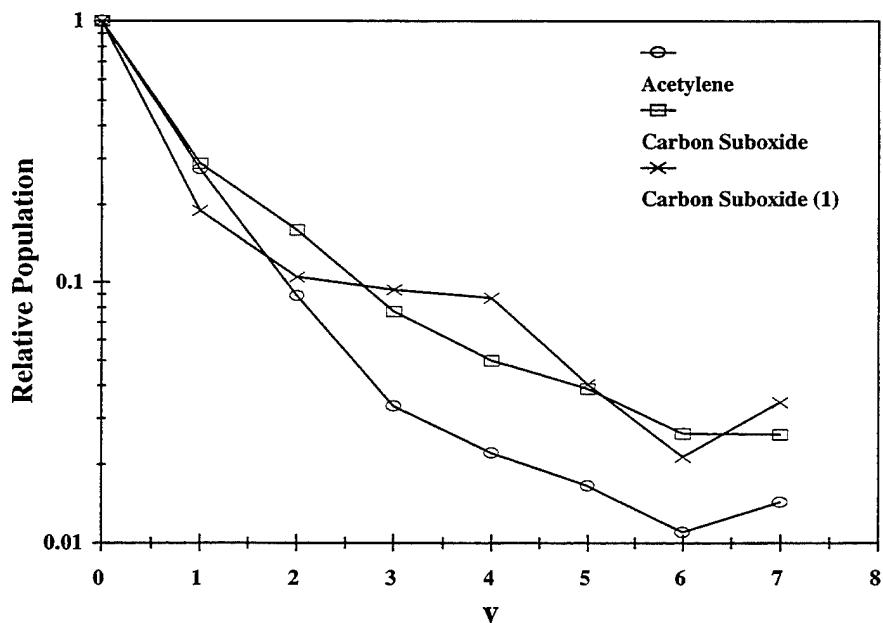

Figure 12. Relative vibrational state populations of CO(d) typical of the 473–873 K temperature range. The carbon suboxide fuel yields a slightly hotter vibrational state distribution than the acetylene. "Carbon suboxide (1)" refers to the result at room temperature with the view port 1 cm downstream of the injection point.
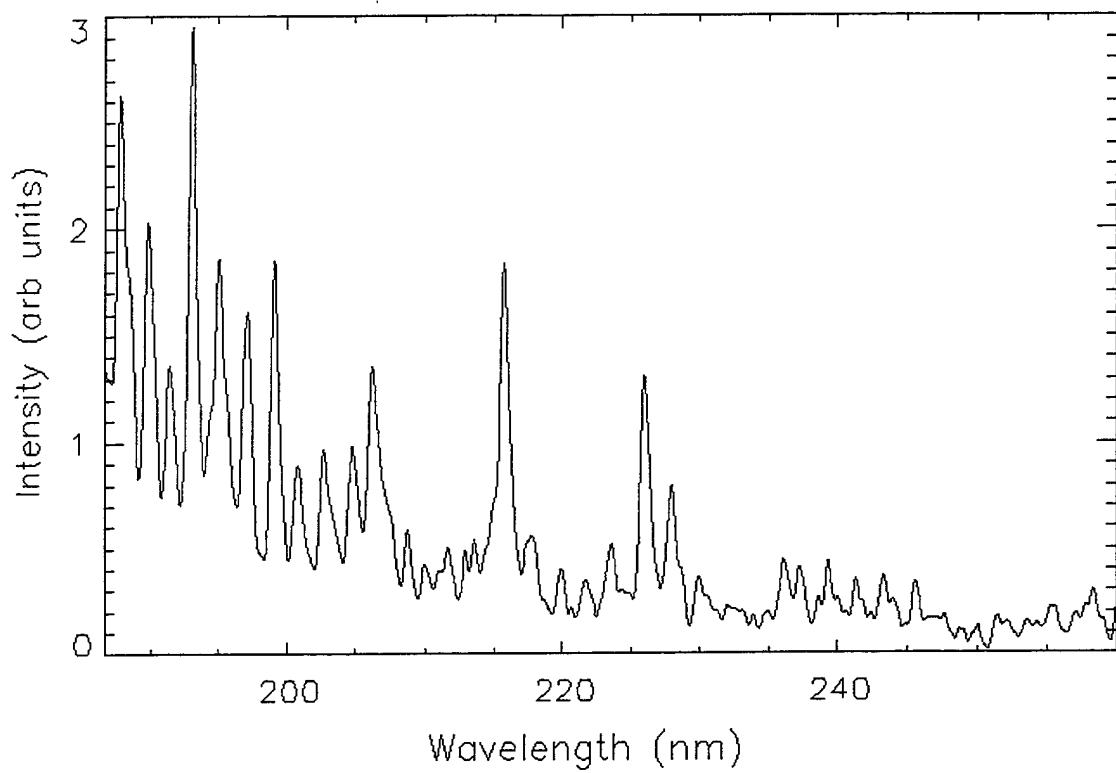
Figure 13. Ultraviolet C_3O_2 + O chemiluminescence spectrum with fuel injector 1 cm upstream of spectrometer viewing region. Flowtube temperature is 295 K. The spectrum has been corrected for spectrometer sensitivity.
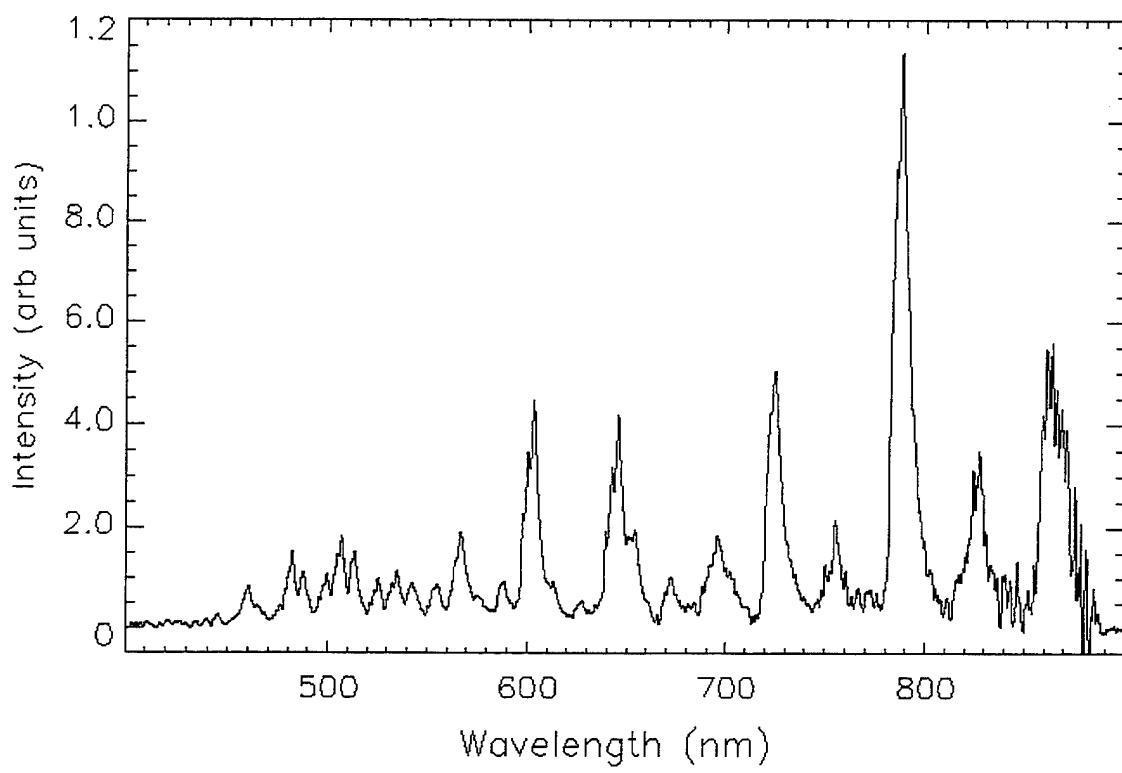
Figure 14. Visible/near-IR C_3O_2 + O chemiluminescence spectrum with fuel injector 1 cm upstream of spectrometer viewing region. Flowtube temperature is 295 K. The spectrum has been corrected for spectrometer sensitivity.

reaction (3b). There may be fuel-rich regions near the injector that allow other chemical paths to CO* to contribute to the emission. These observations indicate that some caution should be exercised when quantitatively comparing data from other flow systems to those obtained with the FFDS system.

3.4. Other Fuels

Chemiluminescence resulting from O atom reaction with several other fuels was also investigated, including methane, ethane, and ethylene. Tjossem and Cool have reported the detection of the C_2O radical in several light hydrocarbon/O_2/Ar flames at low pressures using multiphoton ionization techniques (Ref. 2). Based on the presence of C_2O, the detection of CO* emissions from these fuels might reasonably be expected, although to our knowledge, these emissions have not been previously reported, at least under very fuel-lean conditions. Due to the weakness of the observed emissions, our experiments were largely confined to monitoring the intensities of the Cameron (0,1) and (0,2) bands as a function of fuel concentration and temperature, although a full spectrum of an ethylene flame was taken at 473 K and is shown in Figures 15 and 16. The ethylene flame chemiluminescence spectrum has relatively poor signal to noise, but the Cameron bands demonstrate a very similar CO(a) state distribution to that of the acetylene and carbon suboxide fuels. No flame emission was visually observed with any of these fuels at any temperature investigated, which is consistent with the spectral data, i.e., the lack of Triplet, Herman, or CH($A \rightarrow X$) emissions. The Asundi (4,0) and (5,0) bands are clearly visible, although the CO(e) emissions appear to be absent entirely. The CO* formed in the C_2H_4 + O system thus appears to be less energetic than that formed in the C_2H_2 + O and C_3O_2 + O systems. A colder electronic and vibrational state distribution may indicate species generated via heterogeneous reactions, since thermalization would be more probable in that case. It may also indicate a lower energy precursor for the C_2O radical, or that CH or CH_2 are the precursors to CO*, since the reaction of CH or CH_2 should not liberate enough energy to form CO(e) or higher vibrational levels of CO(d). Other lower energy reactions that might be indicated by the cooler electronic and vibrational distribution of the C_2H_4 + O system are the reactions, $C_2 + O_2 \rightarrow CO + CO^*$ and $C_2H + O_2 \rightarrow CO^* +$ products. Also observed is a relatively strong emission from the O_2 $b \rightarrow X$ (0,0) transition, which was not observed in the acetylene spectra and may not be strongly quenched by ethylene, and a few argon emission lines beyond 830 nm that were not completely removed during the baseline subtraction.
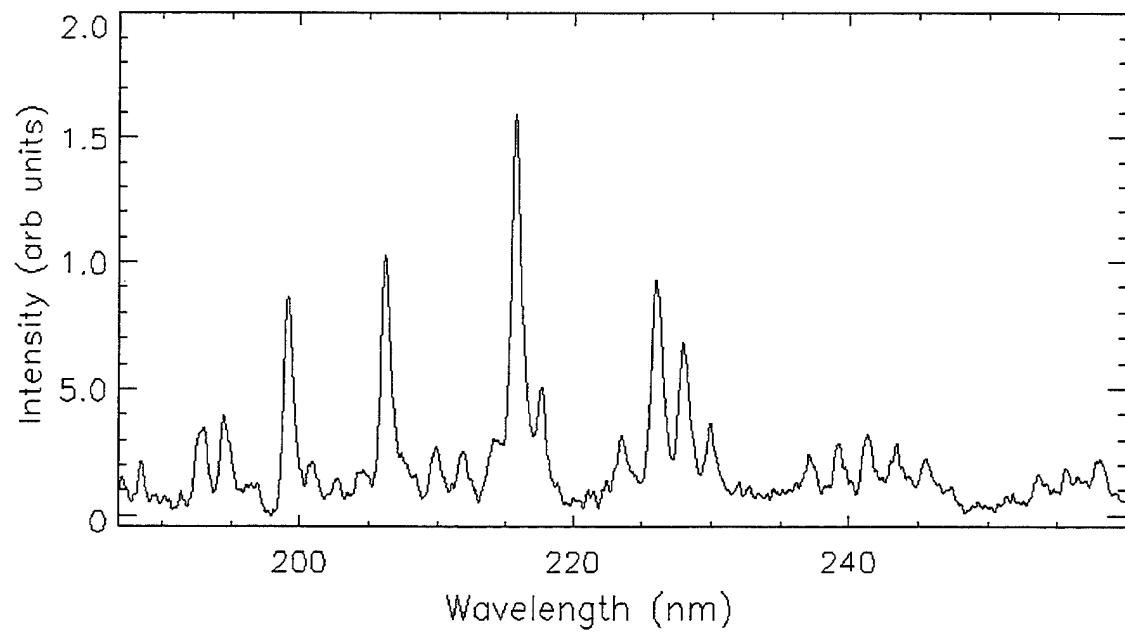
Figure 15. Cameron band emission from an ethylene flame at 473 K. Peak intensity distributions are very similar to $C_3O_2 + O$ and $C_2H_2 + O$ flame spectra shown in Figures 7 and 3, respectively.
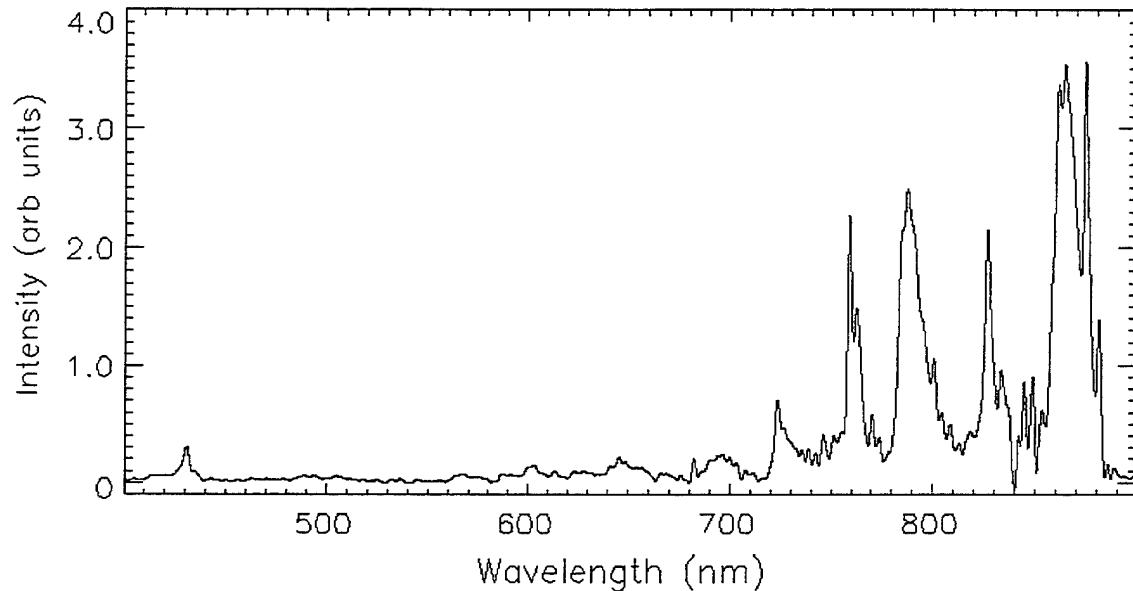

Figure 16. Visible/IR portion of spectrum from an ethylene flame at 473 K. The Asundi (4,0) and (5,0) bands are clearly visible, and traces of Triplet emissions can also be seen.

The temperature and fuel concentration behavior of the Cameron band spectra from O atom flames was similar for methane, ethane, and ethylene fuels. As with previous data, all spectra have background spectra (taken immediately after each run with the fuel off) subtracted to rule out contributions from residual species in the FFDS. Cameron bands could only be observed over limited fuel flow and temperature ranges. The fuel flow ranges over which Cameron bands were observed were fairly constant among the aforementioned fuels; however, the temperature ranges were highly variable from fuel to fuel. The temperature range over which Cameron bands were observed was narrowest for methane (from 673 to 873 K) and widest for ethylene, with traces of Cameron bands observed down to 373 K. Figure 17 shows relative band intensity data taken for these fuels. It can be seen that the Cameron band intensities of all the fuels peak at a fuel:O ratio of about 1:10, then fall off sharply. This is in contrast to the acetylene fuel, which continues to increase nearly linearly over the fuel concentration range investigated. Varying the fuel flows yielded a reaction order between 0.3 and 0.6 for these three fuels.
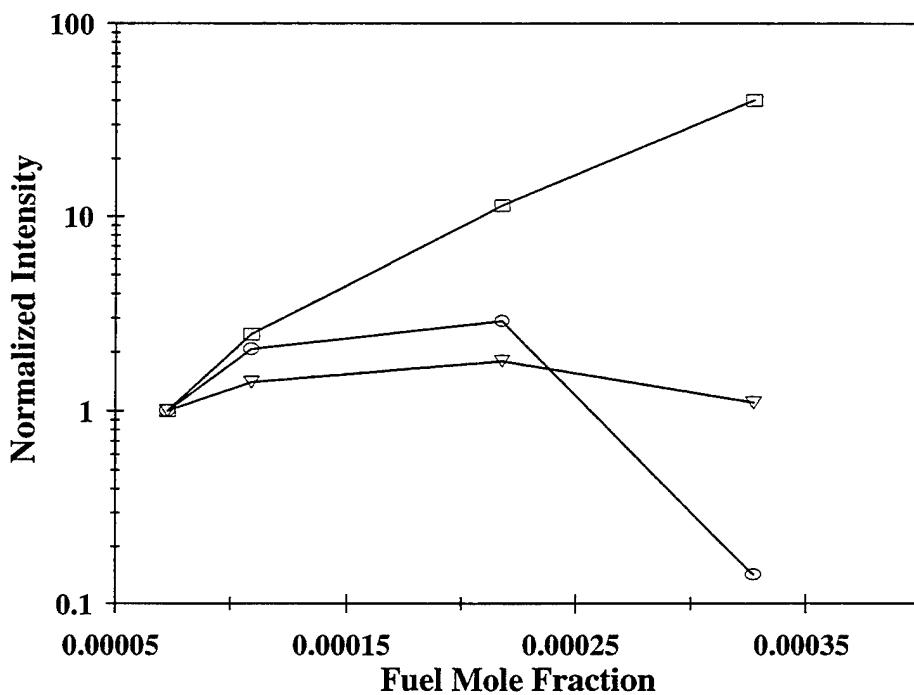
Figure 17. Normalized relative Cameron band intensity as a function of fuel partial pressure for three fuels: C_2H_2 (box), C_2H_4 (circle), and C_2H_6 (triangle). The O atom mole fraction was 0.002, with total pressure of 3 Torr and temperature of 700 K.

4. Summary and Conclusions

The FFDS technique has been applied to the characterization of the CO* triplet state emissions from $C_2H_2 + O$ and $C_3O_2 + O$ flames from room temperature to nearly 900 K. The similarity of the carbon suboxide and acetylene flame spectra is consistent with previous work, where it was concluded that C_2O is the main precursor to CO* in both systems.

Since the activation temperature we have measured for the production of each of the different CO triplet states in acetylene flames is very close to that published for the reaction, $C_2H_2 + O \rightarrow$ products, it is concluded that the overall production rate for CO* is controlled by the initial reaction step and that branching to the different triplet states of CO in subsequent steps is relatively temperature independent. This probably indicates that the main CO* production channel involves the $C_2O + O$ reaction step throughout the temperature range, as appears to be the case at room temperature (Ref . 1).

The observed activation temperature for production of the CO triplet states in C_3O_2 flames was found to be much greater than the value for the reaction, $C_3O_2 + O \rightarrow$ products, which is known at moderate temperatures. This result suggests that the minor reaction branch that produces C_2O has a higher activation energy than the major branch of the total reaction. The activation temperature for the reaction, $C_3O_2 + O \rightarrow C_2O + CO_2$, would be ~ 2700 K by this interpretation, compared with ~1070 K for the total reaction, $C_3O_2 + O \rightarrow$ products.

The same CO* band systems (Cameron, Asundi, Herman, and Triplet) were seen with both C_2H_2 and C_3O_2 fuels, although the CO a', d, and e state populations appeared vibrationally hotter for C_3O_2. In addition, stronger $CO(A{\rightarrow}X)$ bands were seen in the C_3O_2 flame. The CO(A) state may be populated by collisionally induced intersystem crossing from more energetic triplet CO produced in the C_3O_2 flame. The more energetic CO* may be attributable to the higher exothermicity of the $O + C_3O_2$ reaction as compared to the exothermicity of the reactions that produce C_2O in the C_2H_2 flame. The resulting hotter vibrational population of the C_2O would make additional energy available for the excitation of CO in the subsequent $C_2O + O$ reaction. The most striking similarity in emission features for the two fuels was the $CO(a{\rightarrow}X)$ Cameron band system. The relative peak heights and band progression cutoffs within the Cameron band manifold appeared identical for the two fuels, except where perturbed by overlap with CO Fourth Positive $(A{\rightarrow}X)$ bands below about 200 nm. Larger differences between the spectra from

31

these two fuels were seen in the band systems radiating in the visible and near-IR portions of the spectrum.

Several other fuels were briefly investigated, including ethylene, ethane, and methane. Cameron band emission was observed with all of these fuels at elevated temperature, and was strongest for ethylene. A full spectrum obtained for an ethylene flame demonstrated similar spectral features to acetylene and carbon suboxide flame spectra, but the nascent CO* appeared to have a less energetic electronic state distribution. It was not clear whether the Herman bands were present in this spectrum or not, but C_2O has been detected by other authors in $C_2H_4 + O_2$ flames (Ref. 2), which may suggest the presence of C_2O here. This would in turn suggest that Herman bands were present but undetected in our C_2H_4 experiments.

The differences in the CO* vibrational state populations in flames with all of the different fuels examined in this study might be construed to indicate that different precursors are responsible for the production of CO*. If such were the case, then the vibrational population distributions would suggest at least three different precursors, corresponding to at least three qualitatively different nascent triplet CO distributions. On the other hand, the differences may be due entirely to differences in the internal energy of a single precursor (i.e., C_2O), produced by different pathways in the different fuel systems.

In acetylene flames, the relative emission intensities of the triplet systems are constant from room temperature to over 600 K, suggesting that a single reaction pathway dominates the CO* chemistry for acetylene. If other reaction pathways were activated at high temperatures, it is likely that the relative band system intensities would change with increasing temperature. Thus, the overall production rate of CO* is controlled by the initial $C_2H_2 + O$ reaction step, and the temperature independence of the partitioning of state populations indicates relatively constant branching ratios in subsequent reaction steps throughout the temperature range. The similar distribution of CO triplet states in the carbon suboxide flame, where C_2O must be the source of CO*, suggests that C_2O plays a dominant role in the production of CO* emissions with both fuels.

References

1. M. L. Burke, W. L. Dimpfl, P. M. Sheaffer, P. F. Zittel, and L. S. Bernstein, *J. Phys. Chem.* **100**, 138 (1966).

2. P. J. H. Tjossem and T. A. Cool, *Proc. of the 20th Intl. Symp. on Combustion,* The Combustion Institute, Pittsburg, PA, 1985.

3. F. F. Marmo, J. Pardur, and P. Warneck, *J. Chem. Phys.* **47**, 1438 (1966).

4. K. H. Becker and K. D. Bayes, *J. Chem. Phys.* **48**, 653 (1968).

5. J. Peeters, W. Boullart, and I. Langhans, *Int. J. Chem. Kinetics* **26**, 869 (1994).

6. K. H. Becker, O. Horie, V. H. Schmidt, and P. Wiesen, *Chem. Phys. Lett.* **90**, 64 (1982).

7. A. Fontjin and S. E. Johnson, *J. Chem. Phys.* **59**, 6193 (1973).

8. C. Pilz and H. Wagner, *Z. Phys. Chem. (Frankfurt)* **NF 92**, 323 (1974).

9. D. G. Williamson and K. D. Bayes, *J. Am. Chem. Soc.* **89**, 3390 (1967).

10. K. Schofield, *J. Phys. Chem. Ref. Data* **8**, 723 (1979).

11. W. B. DeMore et al., *Chemical Kinetics and Photochemical Data for use in Stratospheric Modeling*, JPL Publication 92-20, Jet Propulsion Laboratory, Pasadena, CA (1992).

12. W. G. Mallard, F. Westley, J. T. Herron, R. F. Hampson and D. H. Frizzel, *NIST Chemical Kinetics Database: Version 6.0*, NIST, Gaithersburg, MD, 1994.

13. K. P. Huber and G. Herzberg, *Molecular Spectra and Molecular Structure, Vol. 4, Constants of Diatomic Molecules*, Van Nostrand Reinhold, New York, 1979.

TECHNOLOGY OPERATIONS

The Aerospace Corporation functions as an "architect-engineer" for national security programs, specializing in advanced military space systems. The Corporation's Technology Operations supports the effective and timely development and operation of national security systems through scientific research and the application of advanced technology. Vital to the success of the Corporation is the technical staff's wide-ranging expertise and its ability to stay abreast of new technological developments and program support issues associated with rapidly evolving space systems. Contributing capabilities are provided by these individual Technology Centers:

Electronics Technology Center: Microelectronics, VLSI reliability, failure analysis, solid-state device physics, compound semiconductors, radiation effects, infrared and CCD detector devices, Micro-Electro-Mechanical Systems (MEMS), and data storage and display technologies; lasers and electro-optics, solid state laser design, micro-optics, optical communications, and fiber optic sensors; atomic frequency standards, applied laser spectroscopy, laser chemistry, atmospheric propagation and beam control, LIDAR/LADAR remote sensing; solar cell and array testing and evaluation, battery electrochemistry, battery testing and evaluation.

Mechanics and Materials Technology Center: Evaluation and characterization of new materials: metals, alloys, ceramics, polymers and composites; development and analysis of advanced materials processing and deposition techniques; nondestructive evaluation, component failure analysis and reliability; fracture mechanics and stress corrosion; analysis and evaluation of materials at cryogenic and elevated temperatures; launch vehicle fluid mechanics, heat transfer and flight dynamics; aerothermodynamics; chemical and electric propulsion; environmental chemistry; combustion processes; spacecraft structural mechanics, space environment effects on materials, hardening and vulnerability assessment; contamination, thermal and structural control; lubrication and surface phenomena; microengineering technology and microinstrument development.

Space and Environment Technology Center: Magnetospheric, auroral and cosmic ray physics, wave-particle interactions, magnetospheric plasma waves; atmospheric and ionospheric physics, density and composition of the upper atmosphere, remote sensing using atmospheric radiation; solar physics, infrared astronomy, infrared signature analysis; effects of solar activity, magnetic storms and nuclear explosions on the earth's atmosphere, ionosphere and magnetosphere; effects of electromagnetic and particulate radiations on space systems; space instrumentation; propellant chemistry, chemical dynamics, environmental chemistry, trace detection; atmospheric chemical reactions, atmospheric optics, light scattering, state-specific chemical reactions and radiative signatures of missile plumes, and sensor out-of-field-of-view rejection.